

Tunable optical sectioning in confocal microscopy by use of symmetrical defocusing and apodization

Manuel Martínez-Corral, Marek Kowalczyk, Carlos J. Zapata-Rodríguez, and Pedro Andrés

We present two novel optical methods to achieve a significative improvement in the optical-sectioning capacity of confocal scanning microscopes. The techniques, whose real power is the simplicity with which they can be implemented, consist of a suitable combination of symmetrical defocusing with two different manners of apodizing both parts of the confocal architecture. It is shown that the proposed techniques are useful in both the bright-field and the fluorescence modes and for reflection and transmission geometries. © 1998 Optical Society of America

OCIS codes: 180.1790, 220.1230, 100.6640.

1. Introduction

The most important advantage of confocal scanning microscopy (CSMy) over conventional microscopy is its optical-sectioning capacity.¹ Optical sectioning refers to the attenuation of scattered and reflected light from parts of the object not in the focal plane, thus enhancing the visibility of details of interest. Thus the sectioning capacity is important because it permits the observation of three-dimensional (3-D) objects.

Over the past few years several efforts have been undertaken to improve the two-point resolution of confocal scanning microscopes (CSM's) in the transverse direction.²⁻⁷ However, the irradiance point-spread function (IPSF) is a volume element with an axial extent that, depending on the numerical aperture, is approximately 3 times higher than the radial extent. Thus the axial resolution is one third or less than that in the lateral direction. Therefore the enhancement of the axial resolution of CSM's has always been of considerable interest. As in the transverse direction, the axial two-point resolution can be defined in terms of the Rayleigh criterion.⁸

Therefore two points are separated axially only if they are far enough apart to display an approximately 26% dip between the peaks of their corresponding irradiance patterns. An alternative criterion for comparing the axial resolutions of various systems is the full width at half-maximum (FWHM) for the axial IPSF. This figure, which is closely related to the Rayleigh criterion, is used widely in both analytical and experimental studies. Several methods for enhancing the axial resolution by a narrowing of the FWHM were recently suggested. In this context the use of binary filters composed of one⁹ or two¹⁰ annuli has provided interesting results. A different approach to this problem, the so-called 4Pi confocal architecture,¹¹ is based on the coherent illumination of the fluorescent sample from both sides. This interference process in combination with point detection leads to a great narrowing of the central lobe of the axial IPSF. However, this improvement cannot easily be exploited because of the great strength of the axial sidelobes.

Another approach for increasing the axial two-point resolution, specifically in the fluorescence mode, is the so-called confocal theta-microscopy technique.¹² This technique, which is based on detection orthogonal to the illumination axis, permits the reduction of the dimensions of the central lobe of the axial IPSF by a factor of approximately 3 or even more if the confocal system is apodized with annular apertures.¹³

In this paper we present an optical method for improving the sectioning capacity of CSM's. The technique is useful in bright-field and fluorescence CSM's and for reflection and transmission geome-

M. Martínez-Corral (manuel.martinez@uv.es), C. J. Zapata-Rodríguez, and P. Andrés are with the Departamento de Optica, Universidad de Valencia, E-46100 Burjassot, Spain. M. Kowalczyk is with the Institute of Geophysics, Warsaw University, Pasteura 07, 02-093 Warsaw, Poland.

Received 13 November 1997; revised manuscript received 24 April 1998.

0003-6935/98/296914-08\$15.00/0

© 1998 Optical Society of America

tries. Our approach is based on suitably apodizing and symmetrically defocusing the two arms of the confocal architecture. It is shown that, by the combination of an adequate binary axially superresolving apodization with variable symmetrical defocusing, the width of the central lobe of the axial IPSF can be tuned. This width can indeed be reduced by a factor 2 with no significant increase in the strength of the secondary lobes, which is quite important for axial superresolution in the sense of the Rayleigh criterion.

In many situations stacked object layers must be separated. To quantify the axial resolution of planes perpendicular to the optical axis it is necessary to calculate the response of the system to an axially scanned thin planar fluorescent layer. We show below that the proposed method provides a significant narrowing of the FWHM of such a response. Therefore we conclude that the technique allows an important increase in the optical-sectioning capacity for 3-D information.

In a further step we present a new kind of axial apodization that is specifically suited to combination with symmetrical defocusing in CSM's. What we call destructive-interference apodization provides an axial response with zero at the focal point but twin narrow sidelobes. We show that, by the combination of this apodization with adequate symmetrical defocusing, a considerable improvement in optical-sectioning capacity can be obtained.

In Section 2 we analyze the effect of symmetrically defocusing both parts of the confocal architecture on the axial resolution of the device. In Section 3 we show that adequate combination of symmetrical defocusing with a proper axially superresolving apodization permits the optimization of the sectioning capacity of CSM's. In Section 4 we present a novel, to our knowledge, type of axial apodization—destructive-interference apodization—and show that its combination with symmetrical defocusing provides a quite good optical-sectioning capacity.

2. Symmetrical Defocusing

Let us start by considering the axial IPSF of a CSM after we consider cylindrical symmetry, that is¹

$$I(v = 0, W_{20}) = |h_1(v = 0, W_{20})|^2 |h_2(v = 0, W_{20})|^2, \quad (1)$$

where it is assumed that the pupil functions of the two arms of the confocal setup have the same radial extent. In Eq. (1) v corresponds to the transverse coordinate expressed in optical units, whereas the axial position is specified in terms of the well-known

defocus coefficient W_{20} measured in units of wavelength. Furthermore,

$$h_1(v = 0, W_{20}) = 2 \int_0^1 p_1(\rho) \exp(i2\pi W_{20}\rho^2) \rho d\rho \quad (2a)$$

represents the axial-amplitude point-spread function (PSF) of the illuminating system, where $p_1(\rho)$ is the pupil function, whereas

$$h_2(v = 0, W_{20}) = 2 \int_0^1 p_2(\rho) \exp(\pm i2\pi W_{20}\rho^2) \rho d\rho \quad (2b)$$

represents the axial-amplitude PSF of the collecting set. The upper and lower signs correspond to the reflection and the transmission architectures, respectively.

Equations (2) can be rewritten in the form of a one-dimensional (1-D) Fourier transform if we perform the following geometrical mapping:

$$\zeta = \rho^2 - 0.5, \quad q(\zeta) = p(\rho). \quad (3)$$

If we now substitute Eq. (3) into Eqs. (2), we find that, except for an irrelevant premultiplication phase factor, the individual axial-amplitude PSF's can be described by

$$h_1(v = 0, W_{20}) = \int_{-0.5}^{0.5} q_1(\zeta) \exp(i2\pi W_{20}\zeta) d\zeta, \quad (4a)$$

$$h_2(v = 0, W_{20}) = \int_{-0.5}^{0.5} q_2(\zeta) \exp(\pm i2\pi W_{20}\zeta) d\zeta. \quad (4b)$$

For the case of two circular pupils we have $q_1(\zeta) = q_2(\zeta) = \text{rect}(\zeta)$, and the axial IPSF is given, according to Eqs. (1) and (4), by

$$I(v = 0, W_{20}) = \text{sinc}^2(W_{20}) \text{sinc}^2(W_{20}) = \text{sinc}^4(W_{20}). \quad (5)$$

In comparison with the axial IPSF of a conventional microscope, the CSM's axial IPSF has suffered a 27% reduction in the FWHM and a 95% attenuation in the strength of the secondary lobes. Thus an important effect of two-point axial superresolution is achieved.

The two-point axial-resolution capacity of CSM's can easily be increased by a quite simple technique that takes advantage of the multiplicative character of the axial IPSF. The technique consists of symmetrically defocusing the two parts of the confocal architecture. In fact, the effect of symmetrical defocusing on the response of the system was already

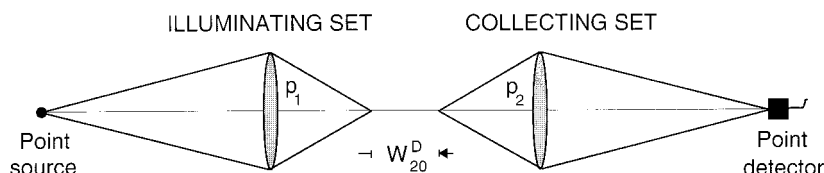


Fig. 1. Schematic layout of a symmetrically defocused transmission-mode CSM. The defocus parameter W_{20}^D gives a measure of the axial shifting of the focal points.

analyzed by other authors.¹⁴⁻¹⁶ From a practical point of view, symmetrical defocusing can easily be implemented either by a slight, controlled axial shift of the collecting set with respect to the illumination set or simply by a slight, symmetrical axial displacement of both the point source and the point detector. In both cases the displacement implies a symmetrical shift of the focal points, and therefore the system is no longer strictly confocal.

From a mathematical point of view, symmetrical defocusing implies a change in the mapped pupil functions, which are now given by

$$q_1'(\zeta) = q_1(\zeta)\exp\left(i2\pi\frac{W_{20}^D}{2}\zeta\right), \quad (6a)$$

$$q_2'(\zeta) = q_2(\zeta)\exp\left(\mp i2\pi\frac{W_{20}^D}{2}\zeta\right). \quad (6b)$$

The parameter W_{20}^D , which measures the induced longitudinal defocus in units of wavelength, can be either positive or negative (see Fig. 1).

Now the axial IPSP of this architecture is given by the product of two independent individual IPSP's that are axially shifted a distance W_{20}^D , that is,

$$\begin{aligned} I(v=0, W_{20}) &= |h_1'(v=0, W_{20})|^2 |h_2'(v=0, W_{20})|^2 \\ &= \left| \int_{-0.5}^{0.5} q_1(\zeta)\exp\left[i2\pi\left(W_{20} + \frac{W_{20}^D}{2}\right)\zeta\right] d\zeta \right|^2 \\ &\quad \times \left| \int_{-0.5}^{0.5} q_2(\zeta)\exp\left[\pm i2\pi\left(W_{20} - \frac{W_{20}^D}{2}\right)\zeta\right] d\zeta \right|^2 \\ &= \left| h_1\left(v=0, W_{20} + \frac{W_{20}^D}{2}\right) \right|^2 \\ &\quad \times \left| h_2\left(v=0, W_{20} - \frac{W_{20}^D}{2}\right) \right|^2. \end{aligned} \quad (7)$$

In the typical case of two circular pupils it is equal in both the reflection and the transmission architectures to

$$I(v=0, W_{20}) = \text{sinc}^2\left(W_{20} + \frac{W_{20}^D}{2}\right) \text{sinc}^2\left(W_{20} - \frac{W_{20}^D}{2}\right). \quad (8)$$

Equation (8) reveals that the axial IPSP of a nonapodized symmetrically defocused CSM is given by the product of two sinc^2 functions that, independently of the sign of W_{20}^D , are relatively shifted an axial distance of $|W_{20}^D|$ (see, for example, Fig. 2). When the product is performed an axial IPSP in which the width of the central lobe is precisely $\Delta W_{20} = 2 - |W_{20}^D|$ is obtained. In other words, the width of the core is now given by the distance between the first zero at the right-hand side of the axial IPSP shifted to the left and the first zero at the left-hand side of the other axial response. It is then clear that simply by continuous variation of the defocusing parameter

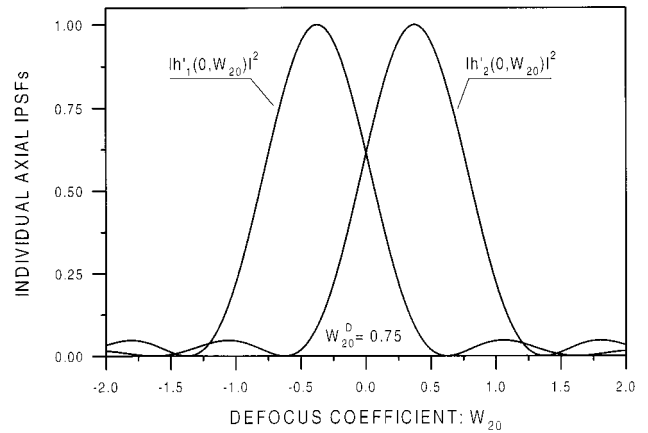


Fig. 2. Axial IPSP's corresponding to the illuminating and the collecting arms of a CSM under symmetrical defocusing of the magnitude of $W_{20}^D = 0.75$.

W_{20}^D , i.e., by gradual symmetrical defocusing of the CSM, it is possible to control at will the width of the axial IPSP core. To illustrate this effect, we have plotted in Fig. 3 the axial IPSP corresponding to some values of the defocusing parameter, including the strictly confocal architecture ($W_{20}^D = 0$). In this figure all the curves are normalized so that their peak value is unity, but in reality the detected irradiance peak drops as symmetrical defocusing increases according to $I(v=0, W_{20}=0) = \text{sinc}^4(W_{20}^D/2)$.

As can be seen from Fig. 3, while the symmetrical defocus increases, the central lobe of the IPSP becomes narrower. However, the relative strength of the sidelobes increases. Note that in this sense values of W_{20}^D higher than unity give rise to very large secondary sidelobes. This fact limits in practice the amount of symmetrical defocusing that can be used and therefore the improvement in two-point axial resolution that can be achieved with this method.

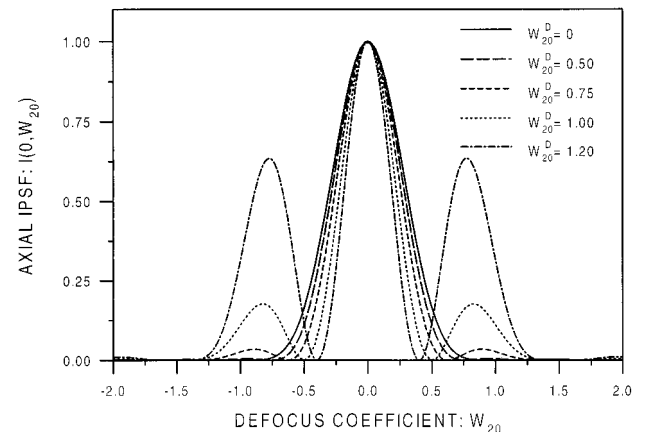


Fig. 3. Normalized axial IPSP corresponding to some symmetrically defocused CSM's. The solid curve corresponds to the strictly confocal architecture.

3. Annular Binary Apodization

As was established in Section 2, the symmetrical-defocusing technique provides a method for obtaining tunable improvement, between certain limits, in the axial resolution of CSM's. However, the technique presents a drawback: the increasing strength of the secondary lobes.

To overcome this drawback, we propose in this section the combination of symmetrical defocusing with using, in both arms of the confocal device, radially symmetric pupil filters that provide axial superresolution. Then we propose using one among the family of filters composed of two transparent annuli of the same area¹⁰ that has a mapped transmittance of

$$q(\zeta) = \text{rect} \left[\frac{\zeta + \frac{1}{2}(1 - \epsilon)}{\epsilon} \right] + \text{rect} \left[\frac{\zeta - \frac{1}{2}(1 - \epsilon)}{\epsilon} \right], \quad 0 < \epsilon < 0.5. \quad (9)$$

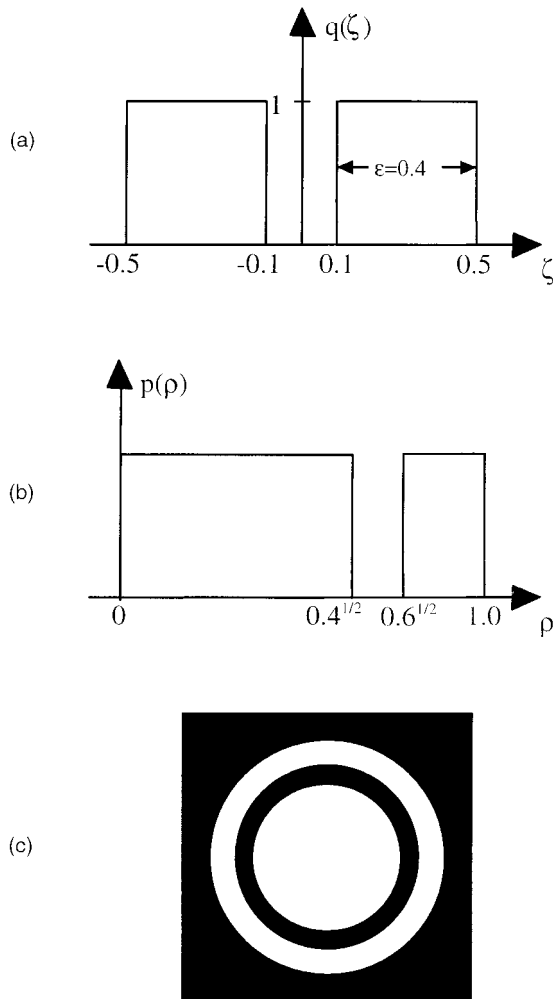


Fig. 4. Member of the family of axially superresolving pupil filters ($\epsilon = 0.4$): (a) ζ -space representation, (b) 1-D representation, and (c) actual 2-D representation.

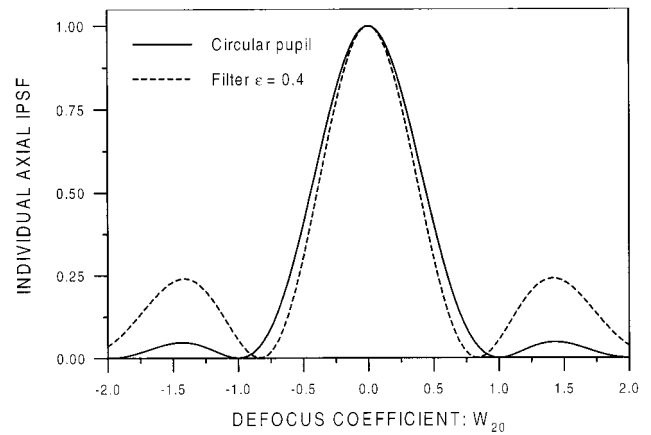


Fig. 5. Axial irradiance pattern corresponding to the filter shown in Fig. 4. As a result of the interference process a quite narrow central lobe is obtained. The solid curve corresponds to the axial response of a circular pupil.

The actual two-dimensional form is represented in Fig. 4.

These filters provide an axial response that is the result of the constructive interference between the waves proceeding through a circular and an annular aperture, both of the same area. Because the waves arrive in phase at the focal point, a narrow axial irradiance peak is obtained (see Fig. 5). This axial-interference process is, in some ways, similar to that produced in the 4π confocal mode.¹¹ Note that, because of the strength of the sidelobes, the use of these filters is not very useful in conventional imaging systems. However, when these filters are placed in a CSM the straightness of the sidelobes is reduced.¹⁰

Next the adequate combination of this apodization with symmetrical defocusing will permit us to obtain a reduction in the strength of the lateral lobes compared with those obtained simply by means of symmetrical defocusing. To illustrate this effect, we show in Fig. 6 the axial IPSF that corresponds to a confocal setup that combines symmetrical defocusing, $W_{20}^D = 2/3$, with the use of a pair of annular filters that have an aperture parameter of $\epsilon = 0.4$. Note from this figure that apodization has achieved a 30% reduction in the strength of the highest secondary lobe.

Thus we can establish that, whereas symmetrical defocusing permits us to tune the width of the central lobe of the irradiance response, the proposed apodization permits us to attenuate the strength of the secondary lobes. Therefore the combination of both techniques attains the effect of tunable axial superresolution.

The axially superresolving properties of the proposed arrangement are represented in Fig. 7. In this figure the irradiance images of two point sources separated by a normalized axial distance d , measured in units of defocus, are shown and compared with those for the strictly confocal setup. The resultant irradiance is summed up on an irradiance basis. In the strictly confocal setup two incoherent

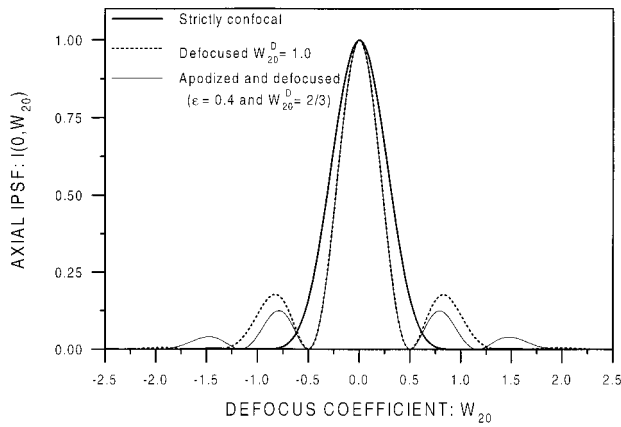


Fig. 6. Normalized axial IPSP corresponding to a suitably apodized, symmetrically defocused confocal device (light solid curve). The parameters of the setup are $\epsilon = 0.4$ and $W_{20}^D = 2/3$. The bold solid curve plots the axial response corresponding to a strictly confocal nonapodized setup, whereas the dashed curve corresponds to the nonapodized but symmetrically defocused system ($W_{20}^D = 1$).

points separated by $d = 0.76$ [Fig. 7(a)] provide an axial-irradiance pattern with a 26% dip. The value of the irradiance in the central minimum is considerably smaller in the proposed apodized and defocused arrangement. The dip between peaks according to the Rayleigh criterion is achieved in the proposed arrangement when the two point sources are axially separated by $d = 0.54$ [Fig. 7(b)]. Therefore a 29% improvement in the axial resolution is achieved.

Up to this point we have analyzed the improvement in the two-point axial resolution that can be achieved with the defocusing technique. However, to make a more complete study on how the optical-sectioning capacity of CSM's is affected by the method, we need to analyze other interesting parameters. In this context it is quite interesting to study

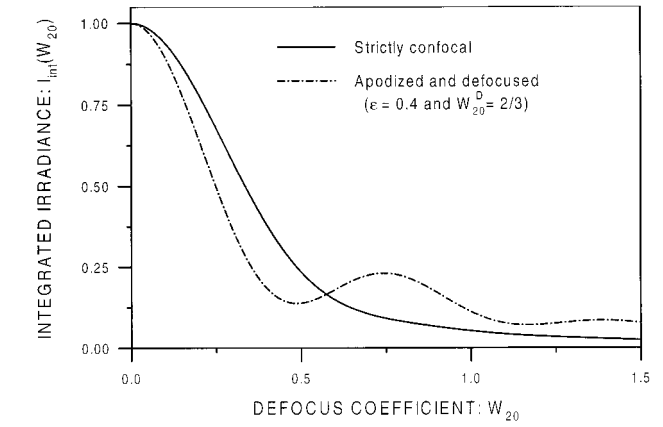
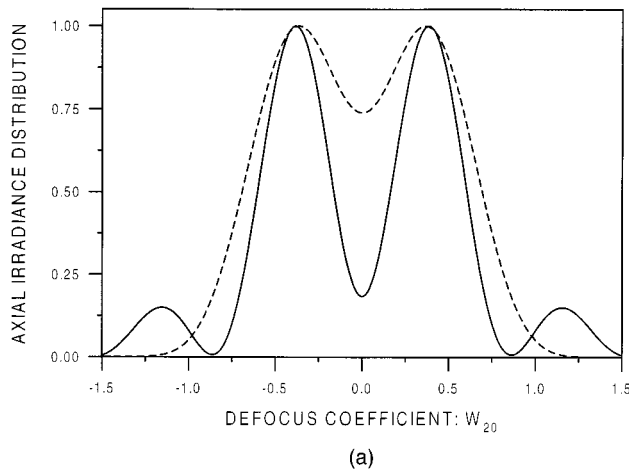


Fig. 8. Integrated-irradiance function corresponding to the setups under study.

the behavior of the so-called integrated-irradiance function, which is defined as¹

$$I_{\text{int}}(W_{20}) = \int_0^{\infty} I(v, W_{20})v dv. \quad (10)$$

This parameter applies equally to the reflection and the transmission geometries and to the bright-field and the fluorescence modes. It gives us information on how the microscope discriminates against different parts of the object not in the focal plane.

In Fig. 8 we represent the integrated irradiance for the setups analyzed in Fig. 6. A 25% gain in sectioning capacity (in terms of the FWHM) is noticeable.

Another quite important parameter, related in this case to the behavior of the system when dealing with planar coherent objects, is the function known historically as $V(z)$. This function is meaningful for only the bright-field reflection mode. It is obtained by evaluation of the irradiance collected by the point

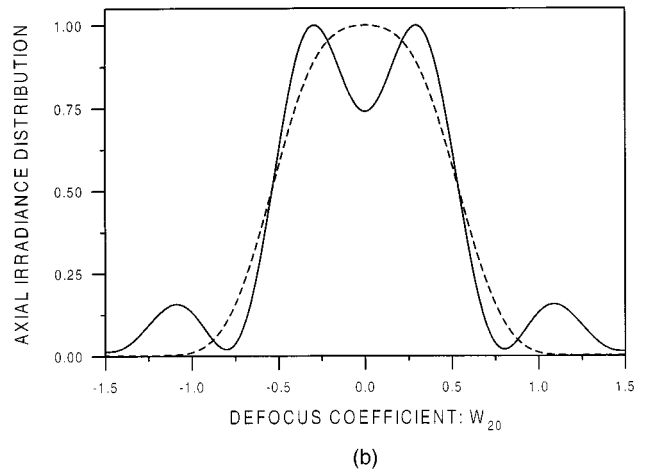


Fig. 7. Irradiance images of two point sources separated by the normalized axial distances (a) $d = 0.76$ and (b) $d = 0.54$. The dashed curves correspond to the strictly confocal arrangement.

detector when a perfect planar reflector that is placed perpendicularly to the optical axis of the setup is scanned axially through the focus. The expression for this function, which we refer to as $I(W_{20})$, is¹

$$I(W_{20}) = \left| \int_{-0.5}^{0.5} q_1'(\zeta)q_2'(\zeta)\exp(i2\pi 2W_{20}\zeta)d\zeta \right|^2. \quad (11)$$

Now, taking into account the expressions for the functions q_i' [see Eqs. (6)] and the transmittance of the filters being binary [see Eq. (9)], we find that

$$\begin{aligned} I(W_{20}) &= \left| \int_{-0.5}^{0.5} q_1(\zeta)q_2(\zeta)\exp(i2\pi 2W_{20}\zeta)d\zeta \right|^2 \\ &= \left| \int_{-0.5}^{0.5} q(\zeta)\exp(i2\pi 2W_{20}\zeta)d\zeta \right|^2. \end{aligned} \quad (12)$$

From Eq. (12) we infer, as indeed was already done by Kimura and Wilson,¹⁴ that symmetrical defocusing does not affect the function $I(W_{20})$. This is because, just when the reflector is at the confocal plane, the point source is imaged onto the detector pinhole. Moreover, because the $I(W_{20})$ curve is given by the squared modulus of the Fourier transform of $q(\zeta)$, it is equal, apart from a scale factor, to that shown in Fig. (5). Note from that figure that the narrowness of the central lobe is accompanied by sidelobes that are much stronger. Hence no improvement in terms of this parameter is achieved.

Finally, we wish to emphasize that the proposed technique barely affects the transverse resolution of the system. This lack of influence occurs for the following reasons: (a) The 3-D IPSF of a lens has an ellipsoidal form. Thus there are not strong differences between its transverse behavior in the focal plane and that in a slightly defocused plane. (b) As demonstrated in Ref. 10, the central lobe of the transverse PSF of an optical system does not spread when the system is apodized by the proposed filter.

4. Destructive-Interference Apodization

In Section 3 an important improvement in the optical-sectioning capacity was achieved by adequate combination of two axially superresolving techniques. Now we propose using a rather different approach. The idea is quite simple, as we show below.

It is seen that, by symmetrically defocusing a CSM, one can select the part of individual axial IPSF's that contributes to the core of the confocal IPSF. Now what we need is an apodization technique that provides an individual axial IPSF with a pair of twin high and narrow lateral lobes. By properly combining both techniques, one can obtain a strong axial-superresolution effect. The apodizer should be selected carefully because it should provide, in addition, a rather weak central lobe. This is because a strong central lobe in individual axial IPSF's gives rise to strong sidelobes in the confocal IPSF obtained after the product. Therefore we propose the use of

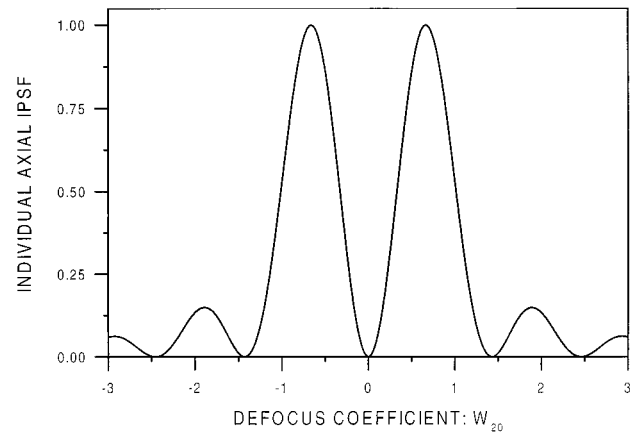


Fig. 9. Axial-irradiance impulse response corresponding to the filter given by Eq. (13). Note that, as a result of the destructive interference between the waves proceeding from the inner and the outer parts of this filter, zero irradiance is achieved at the focus. In addition, the lateral lobes are quite strong and narrow.

destructive-interference apodizers, which provide an axial response with zero irradiance at the focal point.

From among the members of the family of filters with zero focal irradiance we select the one that provides the narrowest slope around zero.¹⁷ The mapped complex-amplitude transmittance of this filter, which can be recognized as the simplest of the so-called Legendre filters,¹⁸ is

$$q(\zeta) = 2\zeta. \quad (13)$$

This filter's axial IPSF can be expressed in terms of the spherical Bessel function of the first order as

$$|h(v = 0, W_{20})|^2 = |j_1(\pi W_{20})|^2. \quad (14)$$

It is plotted in Fig. 9.

Analysis of Fig. 9 shows that an axial pattern with strong, narrow, twin sidelobes and a narrow zero focal irradiance is achieved. Thus the selected apodizer clearly fulfills the imposed requirements. Now, by simply apodizing the two arms of the confocal setup with this filter and applying adequate symmetrical defocusing, we obtain significant narrowness in the core of the axial IPSF.

In Fig. 10 we plotted the axial IPSF that corresponds to a confocal setup that combines destructive-interference apodization with certain symmetrical defocusing. We selected the value of $W_{20}^D = 4/3$ because it permits the left-side maximum of one individual axially shifted IPSF to coincide with the right-side maximum of the other. In this way a strong irradiance peak is achieved. It is then apparent that the proposed technique leads to a high and narrow irradiance peak surrounded by relatively distant and weak secondary lobes, which is quite important in relation to two-point axial resolution.

Also in this case we analyze in Fig. 11 the axially superresolving properties of the method in terms of the Rayleigh criterion. From this figure it is appar-

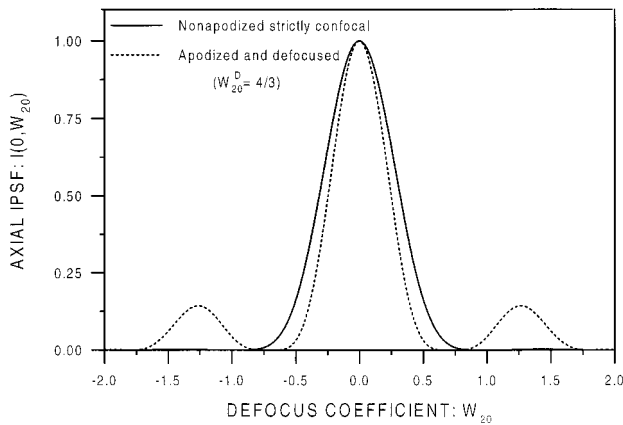


Fig. 10. Normalized axial IPSTF corresponding to a confocal system under destructive-interference apodization and symmetrical defocusing of the magnitude of $W_{20}^D = 4/3$. With the solid curve we have also plotted the axial response corresponding to the strictly confocal, nonapodized setup.

ent that a 24% improvement in the axial two-point resolution is achieved.

Although it can be shown by numerical calculation that the integrated-irradiance function is slightly narrowed, we now prefer to center our attention on the $I(W_{20})$ function. As was shown in Section 3 the $I(W_{20})$ function is given by the squared modulus of the product of the 1-D Fourier transform of the product of the mapped transmittances. In this case, $q_1(\zeta)q_2(\zeta) = 4\zeta^2$. It is easy to recognize that the function $4\zeta^2$ corresponds to the profile of an axially superresolving apodizer, so it will provide a 1-D Fourier transform in which the central lobe has undergone significant narrowing. As in the previous case [see Eq. (13)], the function $4\zeta^2$ can be expanded in terms of the Legendre polynomials¹⁷ and then the function $I(W_{20})$ can

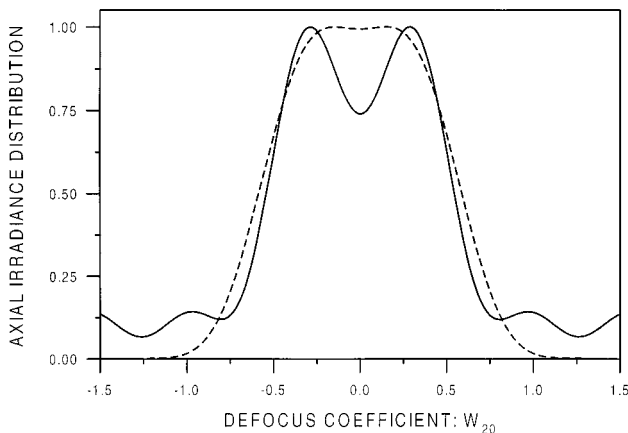


Fig. 11. Irradiance image of two point sources. The points are separated by $d = 0.58$. The 26% dip according to the Rayleigh criterion is obtained. Therefore 24% axial resolution is achieved [see Fig. 7(a)]. The dashed curve corresponds to the strictly confocal arrangement.

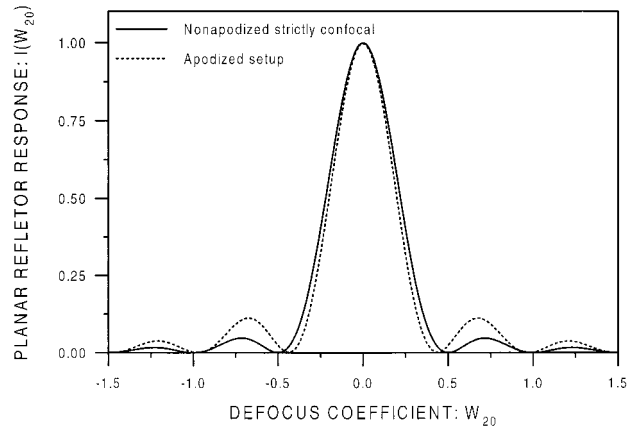


Fig. 12. $I(W_{20})$ function for the same setups that were used for Fig. 10.

be expressed in terms of the spherical Bessel functions as¹⁹

$$I(W_{20}) = \left| \frac{1}{3} j_0(2\pi W_{20}) - \frac{2}{3} j_2(2\pi W_{20}) \right|^2. \quad (15)$$

In Fig. 12 we represent Eq. (15) and the function corresponding to the nonapodized confocal system. A 10% reduction in the FWHM is noticeable. Moreover, in this case the narrowness of the central lobe it is not accompanied by a strong increase in the lateral lobes. Finally, we wish to remark that it can be shown that, also in this case, the transverse resolution is not affected by the proposed technique.

5. Conclusions

We have presented two novel, to our knowledge, optical methods for improving the optical-sectioning capacity of CSM's. The first method successfully combines two axially superresolving techniques: symmetrical defocusing and axially superresolving apodization. The second method incorporates, besides symmetrical defocusing, an apodization technique specifically adapted to confocal architectures: destructive-interference apodization. It has been shown that both methods, which are useful in bright-field and fluorescence CSM, permit the achievement of significant improvements in the optical sectioning capacity.

This study was partially supported by the Dirección General de Investigación Científica y Técnica (grant PB93-0354-C02-01), Ministerio de Educación y Ciencia, Spain. C. J. Zapata-Rodríguez gratefully acknowledges financial support from this institution. M. Kowalczyk gratefully acknowledges financial support by the Komitet Badan Naukowych, Poland (project 8T11F 020 12).

References and Note

1. T. Wilson, ed., *Confocal Microscopy* (Academic, London, 1990).
2. I. J. Cox, C. J. R. Sheppard, and T. Wilson, "Improvement in

- resolution by nearly confocal microscopy," *Appl. Opt.* **21**, 778–781 (1982).
3. Z. S. Hegedus, "Annular pupil arrays. Application to confocal microscopy," *Opt. Acta* **32**, 815–826 (1985).
 4. Z. S. Hegedus and V. Sarafis, "Superresolving filters in confocally scanned imaging systems," *J. Opt. Soc. Am. A* **3**, 1892–1896 (1986).
 5. J. G. Walker, E. R. Pike, R. E. Davies, M. R. Young, G. J. Brakenhoff, and M. Bertero, "Superresolving scanning optical microscopy using holographic optical processing," *J. Opt. Soc. Am. A* **10**, 59–64 (1993).
 6. J. Gromalicki, E. R. Pike, J. G. Walker, M. Bertero, P. Boccaci, and R. E. Davies, "Superresolving masks for incoherent scanning microscopes," *J. Opt. Soc. Am. A* **10**, 1074–1077 (1993).
 7. T. Wilson and S. J. Hewlett, "The use of annular pupil plane filters to tune the imaging properties in confocal microscopy," *J. Mod. Opt.* **37**, 2025–2046 (1990).
 8. R. H. Webb, "Confocal optical microscopy," *Rep. Prog. Phys.* **59**, 427–471 (1996).
 9. C. J. R. Sheppard and M. Gu, "Improvement of axial resolution in confocal microscopy using annular filters," *Opt. Commun.* **84**, 7–13 (1991).
 10. M. Martínez-Corral, P. Andrés, J. Ojeda-Castañeda, and G. Saavedra, "Tunable axial superresolution by annular binary filters. Application to confocal microscopy," *Opt. Commun.* **119**, 491–498 (1995).
 11. S. Hell and E. H. K. Stelzer, "Properties of a 4Pi confocal fluorescence microscope," *J. Opt. Soc. Am. A* **9**, 2159–2166 (1992).
 12. E. H. K. Stelzer and S. Lindek, "Fundamental reduction of the observation volume in far-field light microscopy by detection orthogonal to the illumination axis: confocal theta microscopy," *Opt. Commun.* **111**, 536–547 (1994).
 13. S. Lindek, C. Cremer, and E. H. K. Stelzer, "Confocal theta fluorescence microscopy with annular apertures," *Appl. Opt.* **35**, 126–130 (1996).
 14. S. Kimura and T. Wilson, "Effect of axial pinhole displacement in confocal microscopes," *Appl. Opt.* **32**, 2257–2261 (1993).
 15. C. J. R. Sheppard and D. K. Hamilton, "Edge enhancement by defocusing of confocal images," *Opt. Acta* **31**, 723–727 (1984).
 16. Ho and Shao, "Axial resolution of confocal microscopes revisited," *Optik (Stuttgart)* **88**, 147 (1991).
 17. M. Martínez-Corral, P. Andrés, and J. Ojeda-Castañeda, "On-axis diffractive behavior of two-dimensional pupils," *Appl. Opt.* **33**, 2223–2229 (1994).
 18. J. Ojeda-Castañeda, P. Andrés, and M. Martínez-Corral, "Zone plates with cells apodized by Legendre profiles," *Appl. Opt.* **29**, 1299–1303 (1990).
 19. In Ref. 17 it is shown that, if a 1-D function is expressed in terms of the Legendre polynomials as $t(x) = \sum_{n=0}^{\infty} a_n P_n(x)$, its Fourier transform is given by $\tilde{t}(u) = \sum_{n=0}^{\infty} (-i)^n a_n j_n(\pi u)$. The function $4\zeta^2$ can be expanded in terms of the Legendre polynomials as $4\zeta^2 = (1/3)P_0(\zeta) + (2/3)P_2(\zeta)$. Then the squared modulus of its 1-D Fourier transform is given by Eq. (15).